NANO LETTERS

Letter

pubs.acs.org/NanoLett

Geometric Control of Rippling in Supported Polymer Nanolines

Vijay R. Tirumala,[†,*,∥] Christopher M. Stafford,[‡] Leonidas E. Ocola,[†] Jack F. Douglas,[‡] and L. Mahadevan*[,§]

[†]Center for Nanoscale Materials, Argonne National Laboratory, Argonne, Illinois 60439, United States

[‡]Polymers Division, National Institute of Standards and Technology, Gaithersburg, Maryland 20899, United States

[§]School of Engineering and Applied Sciences, Department of Physics, Harvard University, Cambridge, Massachusetts 02138, United States

Supporting Information

ABSTRACT: We study the swelling behavior of finlike polymer line gratings supported on a rigid substrate and show that the edge-supported polymer laminae undergo a rippling instability with a well-defined ripple wavelength λ transverse to the plane of the solid supporting substrate and a ripple amplitude that monotonically decreases from its maximum at the free-edge. These ripple patterns develop due to inhomogeneous compressive strains that arise from the geometric constraints that progressively suppress swelling near the supporting substrate where the laminae are clamped. By experimentally examining the influence of swelling strain and pattern geometry on the observed rippling instability, we find that the ripple wavelength λ scales with line width w for sufficiently long gratings, which is consistent with a simple theory. These trends were validated for polymer nanoline test patterns having w between (50 to 250) nm and a height-to-width aspect-ratio in the range 0.5 to 5. Our results suggest that line geometry, rather than material properties, governs the onset of rippling and suggest simple rules for their control.

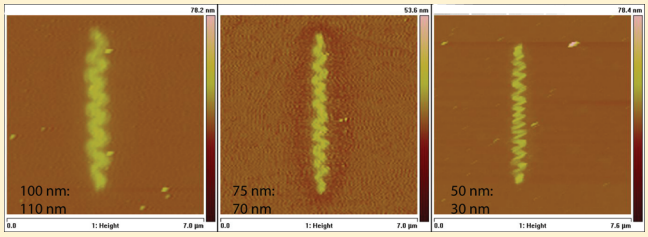

KEYWORDS: *Rippling, polymer, line gratings, hydrogels, nanostructures*

The wrinkling of thin sheets can be induced by a variety of causes: boundary forces, differential growth or shrinkage of one part of the sheet relative to another, or deformation of the sheet relative to a substrate that supports it.[1] In recent years, there has been an explosion of technical activity aimed at exploiting this type of buckling instability for nanofabrication, thin film metrology, and for tuning the elastic properties of thin films,[2−6] as well as in understanding its variegated appearance in problems of biological morphogenesis.[7−10] A particular instance of this mechanical instability arises from the constrained growth of the edge of a long leaf or the plastic deformation induced by stretching on the torn edge of plastic sheets.[9,10] In these cases, the undulations at the free edge of the surface are constrained by a condition that far from the sheet there is no growth or deformation. Patterns with a similar geometry and conforming broadly to these physical conditions are also found frequently in micro- or nanoscale polymer features fabricated using photolithography, electron-beam lithography, or nanoimprint lithography.[11−15] Here we use a minimal setting to explore these patterns in nanoscale systems using a combination of experimental observations and simple theoretical ideas and show that the patterns follow the same general mechanical principles recently unraveled in macroscopic systems. An immediate consequence is the ability to control or suppress these instabilities for practical use.

We use direct-write electron-beam (e-beam) lithography for the precision control of the geometry, degree of cross-linking, swelling, and elastic properties of polymer nanostructures, focusing here on the creation of nanolines with widths in the range of (50 to 250) nm. The lines patterned using e-beam lithography remain irreversibly grafted to the silicon substrate due to the excess generation of secondary electrons in the vicinity of the substrate (see Figure 1a,b for method illustration); that is, the e-beam crosslinks the exposed regions of polymer through the entire depth. This allows us to understand the onset of the mechanical instability observed in response to deformation by swelling or some other means. We chose swelling to induce deformation in polymer line gratings since selective dissolution of photosensitive polymers is a key step in semiconductor fabrication and was shown to strongly influence line-edge roughness.[16−18] Specifically, we use poly(*N*-isopropylacrylamide) (PNIPAm), a widely studied hydrogel that can be cross-linked using focused electron-beam in its dry state to study a mechanical stability in response to swelling in water.[19−22] By simply changing the e-beam exposure time, the absorbed dose, and the extent of cross-linking, we can control the swelling response of PNIPAm.

When immersed in water, the cross-linked PNIPAm nanolines undergo significant swelling. However, irreversible grafting prevents swelling at the substrate interface (supported

Received: December 6, 2011
Revised: February 7, 2012
Published: February 21, 2012

   dx.doi.org/10.1021/nl204306q | *Nano Lett.* 2012, 12, 1516−1521

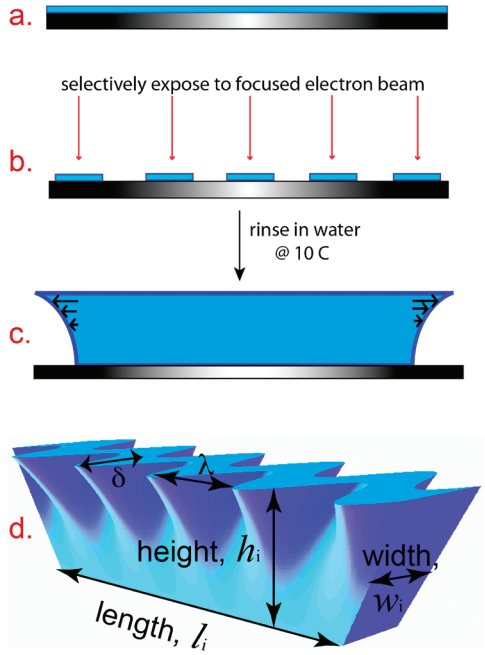

Figure 1. Process steps involved in the fabrication of PNIPAm nanolines using electron-beam lithography include (a) spin-coating a film of desired thickness from aqueous PNIPAm solution, and (b) selective irradiation of the polymer thin film to electron-beam to induce cross-linking in a dry state and removal of unexposed regions by dissolving them in water at 10 °C. (c) The side-view of nanolines after immersion in water, which causes them to undergo substantial swelling at 10 °C while they remain highly grafted without swelling near the substrate. (d) When the swelling strain at the free-edge of nanolines exceeds a critical strain edge rippling ensues with a ripple wavelength λ and maximum in ripple amplitude δ at the free-edge of the nanolines away from the supporting substrate.

edge) and introduces a gradient in swelling through the line height, which translates into longitudinal compression along the free-edge of the lamina (Figure 1c). The longitudinal compression in turn leads to rippling of the patterned PNIPAm nanolines (Figure 1d) whose amplitude decreases monotonically away from the free-edge. While various theoretical frameworks have been put forth to explain these instabilities,[23−25] a clear understanding of the design rules necessary to control this type of rippling instability in patterned polymer nanostructures does not exist.

Scaling Theory. To understand the dependence of characteristic length scales of the rippling instability on material and geometric properties of nanolines, we follow a recent framework that characterizes these rippling instabilities in leaves and other growing laminae.[10] The difference between a polymer nanoline supported by the substrate at one edge and the edge of a long leaf is primarily one of absolute scale. However, the relative scales, that is, the height-to-width and width-to-length aspect ratios are similar in both systems as is the driving mechanism. Whereas the rippling of a leaf edge is driven by the excess growth of the edge, the rippling of a polymer nanoline is driven by the substrate-induced constraint that prevents isotropic swelling. Thus, rippling at the free-edge of a supported polymer lamina and the edge of a long leaf are both driven by the residual nonuniform strain, which allows us to use the same mechanisms to describe the observed instability of polymer nanolines.

We consider a long polymer lamina of length l, width w, and height h ($w \ll h < l$) attached along the long edge to a rigid substrate. In response to a differential swelling strain β that varies along its height, the supported lamina can buckle into a set of periodic ripples of wavelength λ, amplitude δ, and dimensionless wavenumber $k = 2\pi w/\lambda$. This will happen only when the purely compressive mode of the lamina is energetically more expensive than the rippled mode; the transition occurs when the bending and compression energies are of the same order. Matching the bending energy per unit area $Ew^3\delta^2k^4$ with the dimensionless stretching energy per unit area $Ew\beta^{*2}$ then yields a critical swelling strain $\beta^* \sim \delta wk^2$. Since approximate inextensibility of deformed laminae implies that the swelling strain, $\beta^* \sim \delta^2k^2$, we finally find that the critical strain $\beta^* \sim w^2k^2$ and vanishes as the line width vanishes. The finite height of the lamina precludes the wavelength from becoming too large, so that $k \leq 1/h$ and $\beta^* \sim w^2/h^2$. Below this critical strain β^*, the swelling strain is accommodated within the lateral dimensions of lamina without rippling while above it the wavelength of the ripples $\lambda \sim h\beta^{*-1/2}$. When the lamina height is much taller than its width, that is, $w \ll h$, there is only one length in the problem and in this limit, the characteristic wavelength of the instability scales with the width of the lamina. In the other limit, when $h \ll w$ the assumption of a thin plate breaks down and the proposed scaling laws are no longer valid.

Experimental Observations. To understand if these scaling laws allow us to explain the observed experimental results on edge rippling of supported polymer laminae, we consider a supported polymer line of contour length, l, width w, and height, h, in a swollen (rippled) state. The corresponding dimensions in an unswollen state are denoted with a subscript 0. The thickness-dependent swelling strain results in an end-to-end contour length at the top surface of a swollen line different from that in the dry state (l_0). To study the effect of pattern geometry and swelling response, a series of isolated straight lines with systematically varying w_0 in the range of (50 to 250) nm and l_0 in the range of 100 nm to 15 μm were nanofabricated in thin PNIPAm films of systematically varying thickness h_0 in the range of (30 to 180) nm. The swelling response of PNIPAm nanolines was tuned by systematically varying the exposure dose during e-beam lithography in the range (250 to 1500) μC/cm^2. All patterns were fabricated in triplicate to ensure reproducibility of results. The parameters l, wavelength λ, and amplitude δ of ripples are measured directly from real-space atomic force microscopy images of swollen PNIPAm nanolines. The contour length, ripple wavelength, and ripple amplitude of swollen lines are computed using ImageJ image analysis software available from National Institute of Health.[26]

The PNIPAm nanolines can be preserved in a swollen state by flash drying with nitrogen. Figure 2a shows a representative top-view scanning electron micrograph of 250 nm wide PNIPAm lines fully swollen in water at 10 °C and imaged in a dry state. The line width in the swollen state was measured using transmission electron microscopy to be on the order of 650 nm, which is more than twice the designed line width (250 nm) in dry state. PNIPAm is also known to undergo as much as a 10-fold decrease in volume in response to a change in ambient temperature to above (32 to 35) °C.[27−32] Figure 2b shows the top-view scanning electron micrograph of PNIPAm nanolines from Figure 2a after immersion in water at 40 °C and imaged in a dry state. The deswelling of PNIPAm chains at 40 °C is sufficient to recover the originally designed line width.[22] Some residual rippling seems to persist in the patterns shown in

dx.doi.org/10.1021/nl204306q | Nano Lett. 2012, 12, 1516−1521

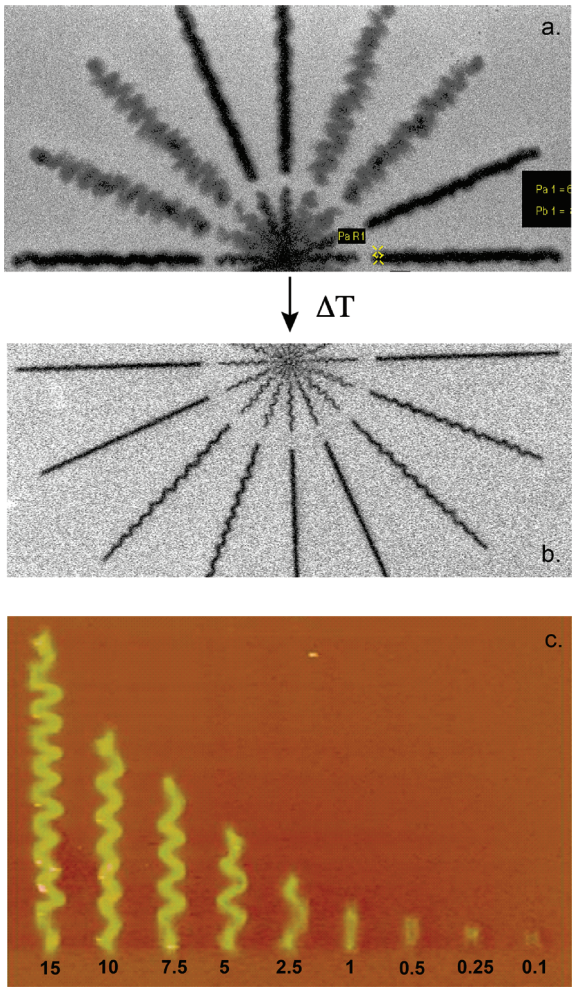

Figure 2. Effect of swelling strain and pattern geometry on the observed rippling instability in PNIPAm nanolines. (a) Representative scanning electron micrograph of rippling instability in swollen PNIPAm nanolines of 250 nm line width, patterned at an exposure dose of 300 $\mu C/cm^2$and imaged in a dry state after immersion in water at 10 °C followed by flash-drying using nitrogen. The line width at the swollen free-edge is measured to be 650 nm. (b) The scanning electron micrograph of deswollen PNIPAm nanolines similar to those in (a) but after immersion in water at 40 °C and flash-dried using nitrogen. Measured line width at the free-edge of PNIPAm nanolines in (b) is 250 nm. (c) Atomic force micrograph of swollen PNIPAm nanolines patterned with 250 nm line width at an exposure dose of 500 $\mu C/cm^2$ and imaged in a dry state after flash-drying. Numbers underneath each line in panel c indicate line length in micrometers.

Figure 2b even after deswelling contrary to that expected from the schematic in Figure 1d. However, high grafting density near the substrate interface is a necessary condition for edge rippling and grafting density is proportional to exposure dose. Consequently, nanolines patterned at low exposure doses (<200 $\mu C/cm^2$) readily detach from the substrate upon swelling and undergo unconstrained lateral expansion whereas those patterned at high exposure doses undergo edge-rippling. None of the patterns considered for this study were detached from the substrate upon swelling and the change in length was largely limited to the free-edge of lines. The effect of pattern geometry on the rippling instability is studied by patterning isolated nanolines of systematically varying length in the range 250 nm to 15 μm. Figure 2c shows a representative atomic force micrograph of fully swollen PNIPAm nanolines patterned at an exposure dose of 500 $\mu C/cm^2$ and imaged in dry state after flash drying. One finds that the rippling instability is remarkably similar in all lines except in cases where it is completely suppressed (length $\leq$1 μm).

In Figure 3, we show the phase space for the response of PNIPAm nanolines as a function of height-to-width (h/w)

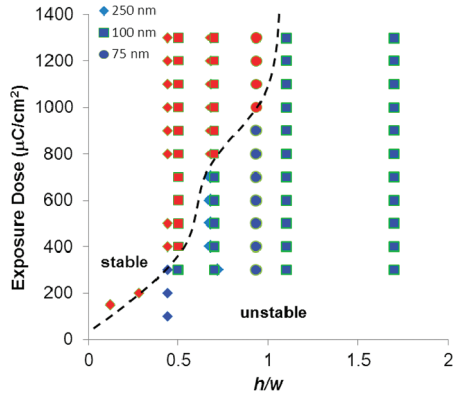

Figure 3. E-beam exposure dose and (h/w) phase space for mechanical stability of swollen PNIPAm nanolines with 75, 100, and 250 nm width patterned at systematically varying exposure dose in the range (100 to 1300) $\mu C/cm^2$ in thin films of thickness ranging between 30 and 180 nm. Dotted line is drawn as a guide to the eye. Markers filled in blue represent rippled nanolines while the same markers filled in red represent stable nanolines.

aspect-ratio and e-beam exposure dose for 75, 100, and 250 nm designed line width and 30, 50, 75, 110, and 170 nm height measured in the dry state nanofabricated at systematically varying exposure dose in the range of (100 to 1300) $\mu C/cm^2$. The dotted line differentiates the region in which the PNIPAm nanolines are stable against rippling from the region in which the instability is prominent. One finds that (i) the features with low (h/w) aspect-ratio are stable against rippling at all exposure doses, (ii) features with modest (h/w) aspect-ratio are susceptible to rippling but only when the exposure dose exceeds that corresponding to a critical swelling strain, and (iii) at high values of (h/w) the lines are unstable at all exposure doses studied. Clearly, the rippling instability is dependent on the swelling behavior, which is governed by cross-link density and temperature, as well as the geometry of PNIPAm nanolines. Validating the experimentally observed dependence of parameters such as the wavelength and amplitude of ripples on the properties of the nanolines is necessary to reduce the parametric space and control this phenomenon.

We quantify the change in ripple wavelength and ripple amplitude as a function of the swelling strain for PNIPAm nanolines where, w_0 = (250, 100, 75, 50 nm), h_0 = (30 to 180) nm, l_0 = (5, 7.5, 10, 15 μm) and patterned using exposure doses in the range, (200 to 750) $\mu C/cm^2$. Together, these set of PNIPAm nanolines correspond to h/w aspect-ratios in the range, (0.5 to 3.5), that is, they cannot always be treated as thin plates, the only limit where our scaling theory applies. Nevertheless, we will see that our theory gives reasonable estimates.

Rippling is suppressed in PNIPAm nanolines of this geometry above 1000 and 750 $\mu C/cm^2$ corresponds to the lowest swelling strain required to trigger the instability. In Figure 4a, we plot the scaled ripple wavelength λ/h (with h being the height of the swollen PNIPAm nanolines) as a

dx.doi.org/10.1021/nl204306q | Nano Lett. 2012, 12, 1516–1521

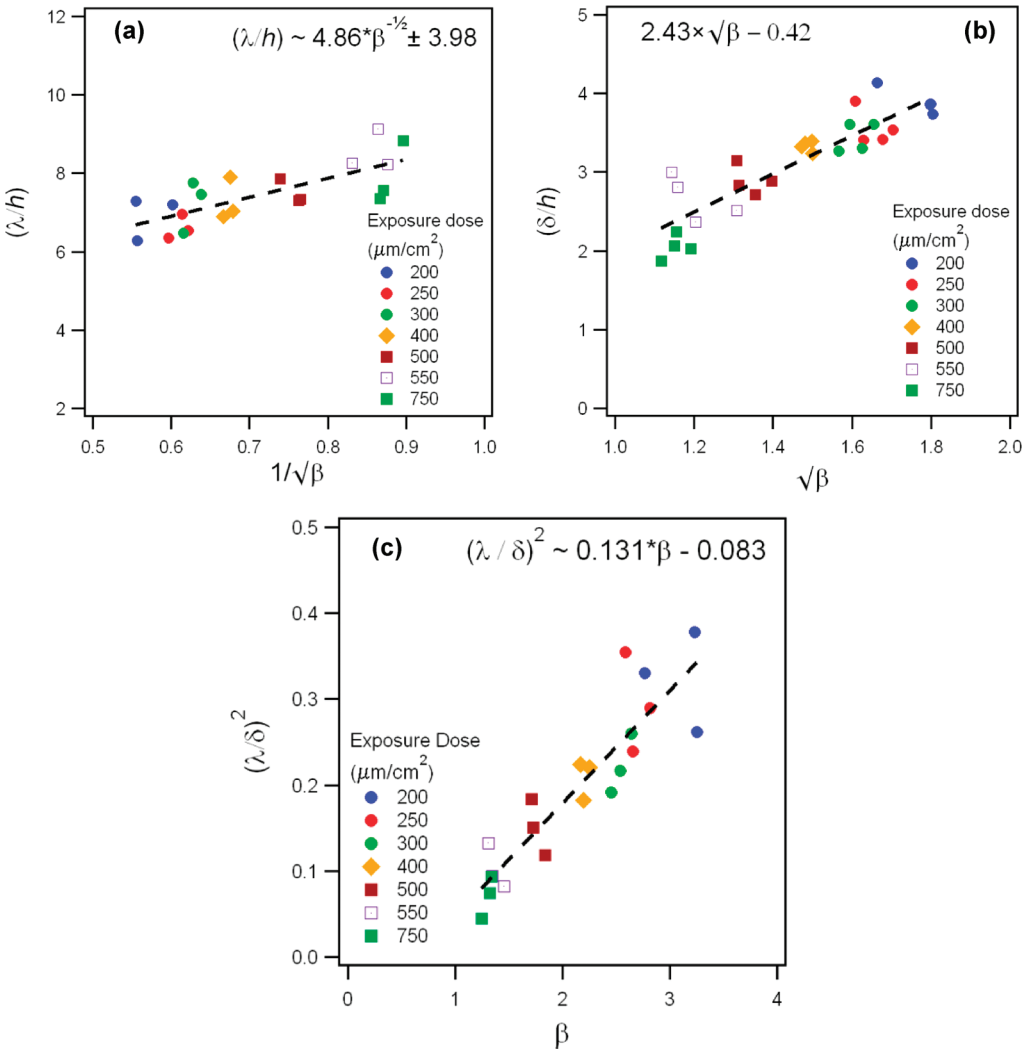

Figure 4. (a) Ripple wavelength and (b) ripple amplitude scaled relative to the swollen height plotted as a function of swelling strain for PNIPAm nanolines of 250 nm line width patterned over a range of exposure doses given in the legend. (c) The dependence of ripple wavelength on ripple amplitude through the swelling strain. The black dotted line in each panel is the best fit of data to the respective equations that describe the respective scaling relations. Uncertainty in the buckling wavelength and amplitude was estimated to be at 5%.

function of swelling strain $\beta > \beta^*$ and find that the linear relation $\lambda/h = 4.86\beta^{-1/2} + 3.98$ agrees with the scaling theory at onset. In Figure 4b, we plot the scaled ripple amplitude δ/h as a function of the swelling strain $\beta > \beta^*$ and find that the linear relation $\delta/h = 2.43\beta^{1/2} - 0.42$ also agrees with the scaling theory beyond the onset of buckling, when inextensibility fixes the amplitude of the ripples. The data collapse for all exposure doses and initial lengths, l_0, suggesting that the simple scaling theory is sufficient to capture the essence of the phenomena. From the scaling relationships, we can deduce a critical swelling strain β^* as the swelling strain corresponding to the intuitively expected condition for the onset of the rippling instability, with $\delta \cong h/2$.[33] From the data of (δ/h) versus β shown in Figure 4a, we compute the value of β^* to be 14.33% for PNIPAm nanolines of 250 nm line width. Assuming isotropic volume change, β^* = 14.33% corresponds to a volumetric swelling degree of 49.5%. In contrast, wrinkling instability occurs in supported PNIPAm thin films when the volume change corresponding to the critical swelling strain approaches 100%.[34] By extrapolation of data plotted in Figure 4a, one also finds that the critical wavelength at the onset of rippling instability is determined to be λ^* (β^* at 14.33%) $\approx$ 4.2 μm, which agrees well with the largest wavelength measured at an $l_0 \approx 2.5$ μm and patterned at an exposure dose of 250 μC/cm^2. At swelling strains far greater than the critical swelling strain, the ripple wavelength reaches a plateau value, λ/h ($\beta \gg \beta^*$) = 3.98, whereas the ripple amplitude continues to increase with swelling strain. In Figure 4c, we plot the rippling wavelength as a function of the amplitude scale and show that this is consistent with the scaling law $\delta \sim \lambda\beta^{1/2}$ outlined above and the detailed calculations of Liang and Mahadevan.[12]

Conclusions. Our study shows that the rippling instability due to the swelling of edge-supported PNIPAm nanolines fabricated using e-beam lithography is influenced rather strongly by the pattern geometry than the material properties such as elastic modulus (see Supporting Information I). This instability is different from other mechanical instabilities observed in polymer thin films such as buckling. It is well-known, for example, that the characteristic wavelength and amplitude of buckling depend on the mechanical properties of both the polymer thin film as well as the substrate supporting it.[2−4] Moreover, the scaling of ripple amplitude and ripple wavelength with swelling strain is similar to that observed in free-edges of leaves and suggests that the phenomenological

dx.doi.org/10.1021/nl204306q | Nano Lett. 2012, 12, 1516−1521

basis for rippling instability is the same at macro- and nanoscale. The proposed scaling arguments reasonably describe the observed phenomenology and obviate the use of more involved computational methods that are necessary to simulate swelling-induced rippling in polymer line gratings.

Perhaps a more surprising finding is that the minimum change in volume necessary to induce rippling instability in PNIPAm nanolines is only 50%. Most amorphous polymers absorb as much as 30% solvent by volume depending on solvent quality and temperature.[35] Line gratings fabricated using polymers with propensity for even modest solvent absorption are thus likely susceptible to edge rippling. While the present study is limited to a relatively elastic solid, the critical swelling strain necessary for rippling of line gratings still has implications for glassy photoresist polymers which undergo swelling prior to dissolution in developer solvents.[36] Edge rippling could thus potentially contribute to line edge roughness, a commonly encountered problem during semiconductor fabrication. Extending the universality of rippling to commercially available photoresist patterns is a good next step to establish the design rules dictating their mechanical stability.

Materials and Methods. *General.* Certain commercial materials and equipment are identified in the paper in order to adequately specify the experimental details. In no case does such identification imply recommendation by the National Institute of Standards Technology nor does it imply that the material or equipment identified is necessarily the best available for the purpose. In all figures, error bars represent one standard deviation of the data and is taken as the uncertainty of the measurement.

Nanofabrication. The polymer lines were nanopatterned using direct-write electron-beam lithography following the procedure described earlier.[23] Briefly, a 200 mmol/L solution of poly(*N*-isopropylacrylamide) was synthesized in-house by free-radical redox polymerization at 20 °C. The solution was first filtered using a 0.25 μm Teflon filter. Deionized water of 17.5 MΩ-cm was used in all experiments. PNIPAm films of dry thickness of 170, 110, 75, 50, and 30 nm were prepared by spin-coating the filtered aqueous solution on to a silicon wafer at spin-speeds ranging from (2000−9000) rpm. The films were vacuum-dried to remove any residual solvent and the film thickness was measured at three different points using an alpha-step 500 profilometer (Tencor Instruments) prior to e-beam lithography. E-beam exposures were performed using the Raith 150 electron-beam writer at a 30 keV accelerator voltage and 40 pA current at the Center for Nanoscale Materials, Argonne National Laboratory. The written features were developed by immersing the samples in a water bath maintained at 10 °C for two minutes. The nanopatterned hydrogels swollen in water were flash-dried using a nitrogen gun to preserve the morphology. To ensure reproducibility and to accurately estimate the uncertainty in measurement, each pattern was written in triplicate and developed simultaneously.

Design Criteria for Nanopatterning. Three different sets of patterns were written in each film. The first set of patterns was designed to address the effect of length on the uniaxial compressive stress generated and comprised lines of variable length but the same width (e.g., 250 nm) and height (e.g., 170 nm). A second set of patterns were designed to establish the effect of line width on the mechanical stability of nanostructures and comprised lines that are 5 μm long but are 250, 100, 75, and 50 nm wide, respectively. The lines were designed to be in isolation to minimize the effect of capillary forces on the swollen shape. For each width, ten lines were drawn by exposing each line to a different dose.

Nanostructure Characterization. The patterned polymer nanolines after swelling were preserved by flash-drying and were imaged in a dry state using a Digital Instruments Dimension 3100 atomic force microscope equipped with Nanoscope IV controller (Veeco Instruments). Lines with 250 nm width and various lengths were imaged at 100 nm resolution to ensure rapid characterization. Lines that are 5 μm long but with variable width were imaged at 25 nm resolution. The resolution in both cases includes tip shape convolution, which was measured from imaging a calibration sample. The ripple wavelength, ripple amplitude, and the contour length of the swollen lines were measured using *ImageJ* software on a stylus-equipped tablet portable computer by tracing the contours.

■ ASSOCIATED CONTENT

Ⓢ Supporting Information

Data presented in supporting documents include (i) the linear swelling strain as a function of exposure dose, and (ii) change in material properties computed from the measured linear swelling strain using the framework of Flory−Rehner theory for polymer networks for PNIPAm lines of 250 nm line width and 180 nm height. This material is available free of charge via the Internet at http://pubs.acs.org.

■ AUTHOR INFORMATION

Corresponding Author

*E-mail: (V.R.T.) vijay.r.tirumala@gmail.com; (L.M.) lm@seas.harvard.edu.

Present Address

[‖]Cabot Corporation, 157 Concord Rd., Billerica, MA 01821-7001.

Notes

The authors declare no competing financial interest.

■ ACKNOWLEDGMENTS

We are grateful to Dr. Ralu Divan for helping with nanofabrication and Dr. Derrick Mancini for useful discussions. Use of nanofabrication facilities at the Center for Nanoscale Materials is supported by the U.S. Department of Energy, Office of Science, Office of Basic Energy Sciences, under Contract No. DE-AC02-06CH11357. Additional support was provided by the Harvard-NSF MRSEC, the Kavli NanoBio Science and Technology Institute at Harvard and the MacArthur Foundation (L.M.).

■ REFERENCES

(1) Cerda, E.; Mahadevan, L. *Phys. Rev. Lett.* **2003**, *90* (7), 074302 1−4..

(2) Volynskii, A. V.; Bazhenov, S.; Lebedeva, O. V.; Bakeev, N. F. *J. Mater. Sci.* **2000**, *35* (3), 547−554.

(3) Volynskii, A. V.; Bazhenov, S. *Euro. Phys. J. E* **2007**, *24* (4), 317−324.

(4) Stafford, C. M.; Harrison, C.; Beers, K. L.; Karim, A.; Amis, E. J.; Van Landingham, M. R.; Kim, H.-C.; Volksen, W.; Miller, R. D.; Simonyi, E. E. *Nat. Mater.* **2004**, *3*, 545−550.

(5) Jiang, H.; Khang, D.-Y.; Song, J.; Sun, Y.; Huang, Y.; Rogers, J. A. *Proc. Nat. Acad. Sci. U.S.A.* **2007**, *104* (40), 15607−15612.

(6) Schweikart, A.; Pazos-Perez, N.; Alvarez-Puebla, R. A.; Fery, A. *Soft Matter* **2011**, *7*, 4093−4100.

(7) Caves, J. M.; Kumar, V. A.; Xu, W.; Naik, N.; Allen, M. G.; Chaikof, E. L. *Adv. Mater.* **2010**, *22* (18), 2041−2044.
(8) Hendricks, T. R.; Lee, I. *Nano Lett.* **2007**, *7* (2), 372−379.
(9) Sharon, E.; Roman, B.; Marder, M.; Shin, G.-S.; Swinney, H. L. *Nature* **2002**, *419*, 579.
(10) Liang, L.; Mahadevan, L. *Proc. Natl. Acad. Sci. U.S.A.* **2009**, *106* (52), 22049−22054.
(11) Heidenreich, R. D.; Kammlott, G. W. *Polym. Eng. Sci.* **1977**, *17* (6), 377−380.
(12) Hill, D. A.; Huang, X.; Bazan, G.; Bernstein, G. H. *J. Appl. Phys.* **1992**, *72* (9), 4088−4094.
(13) Regonda, S.; Aryal, M.; Hu, W. *J. Vac. Sci. Technol., B* **2008**, *26*, 2247.
(14) Alvine, K. J.; Ding, Y.; Douglas, J. F.; Ro, H. W.; Okerberg, B. C.; Karim, A.; Soles, C. L. *Soft Matter* **2009**, *5*, 2913−2918.
(15) DuPont, S. J. Jr.; Cates, R. S.; Stroot, P. G.; Toomey, R. *Soft Matter* **2010**, *6*, 3876−3882.
(16) Reichmanic, E.; Thomson, L. F. *Annu. Rev. Mater. Sci.* **1987**, *17*, 235−271.
(17) Bratton, D.; Yang, D.; Dai, J.; Ober, C. K. *Polym. Adv. Tech.* **2006**, *17* (2), 94−103.
(18) *Micro- and nanopatterning of polymers*; Ito, H., Reichmanis, E, Nalamasu, O., Ueno, T., Eds.; ACS Symposium Series 706; American Chemical Society: Washington, DC, 1998.
(19) Heskins, M.; Guillet, J. E. *J. Macromol. Sci.,Chem.* **1968**, *2* (8), 1441−1455.
(20) Nagaoka, N.; Safrani, A.; Yoshida, M.; Omichi, H.; Kubota, H.; Katakai, R. *Macromolecules* **1993**, *26*, 7386−7388.
(21) Panda, A.; Manohar, S. B.; Sabharwal, S.; Bharadwaj, Y. K.; Majali, A. B. *Radiat. Phys. Chem.* **2000**, *58*, 101−110.
(22) Tirumala, V. R.; Divan, R.; Ocola, L. E.; Mancini, D. C. *J. Vac. Sci. Technol., B* **2005**, *23*, 3124−3129.
(23) Fedorchenko, A. I.; Wang, A.-B.; Mashanov, V. I.; Cheng, H.-H. *J. Mech.* **2005**, *21* (3), 131−135.
(24) Mora, T.; Boudaoud, A. *Eur. Phys. J. E* **2006**, *20*, 119−124.
(25) Cendula, P.; Kiravittaya, S.; Mei, Y. F.; Deneke, Ch.; Schmidt, O. G. *Phys. Rev. B* **2009**, *79*, 085429.
(26) *ImageJ: Image Processing and Analysis in Java*, version 1.44; rsbweb.nih.gov/ij/ (accessed January, 2011).
(27) Hirokoawa, Y.; Tanaka, T. *AIP Conf. Proc.* **1984**, *107*, 203−208.
(28) Wu, C.; Zhou, S. *Macromolecules* **1995**, *28*, 8381−8387.
(29) Wu, J.; Zhou, B.; Hu, Z. *Phys. Rev. Lett.* **2003**, *90* (4), 048304.
(30) Wang, J.; Gan, D.; Lyon, L. A.; El-Sayed, M. A. *J. Am. Chem. Soc.* **2001**, *123* (45), 11284−11289.
(31) Lutz, J.-F.; Akdemir, O.; Hoth, A. *J. Am. Chem. Soc.* **2006**, *128* (40), 13046−13047.
(32) Hirotsu, S.; Hirokawa, Y.; Tanaka, T. *J. Chem. Phys.* **1987**, *87*, 1392−1395.
(33) It is geometrically impossible to define a rippling instability with $\delta \leq w/2$.
(34) Harmon, M. E.; Tang, M.; Frank, C. W. *Polymer* **2003**, *44*, 4547−4556.
(35) Park, G.; Ueberreiter, K. In *Diffusion in Polymers*; Crank, J., Park, G., Eds; Academic Publishers: New York, 1968; pp 140−162.
(36) Rao, A.; Kang, S.; Vogt, B. D.; Prabhu, V. M.; Lin, E. K.; Wu, W.-L.; Muthukumar, M. *Langmuir* **2006**, *22*, 10009−10015.